Coupling of exciton-polaritons in low-Q coupled microcavities beyond the rotating wave approximation

Bin Liu,[1,*] Prabin Rai,[2] John Grezmak,[1] Robert J. Twieg,[2] and Kenneth D. Singer[1,†]

[1]*Department of Physics, Case Western Reserve University, Cleveland, Ohio 44106, USA*
[2]*Department of Chemistry, Kent State University, Kent, Ohio 44242, USA*

We have demonstrated coupling between a pair of ultrastrong light-matter coupled microcavities composed of neat glassy organic dye films between metallic (silver) mirrors at room temperature. Based upon our modified coupled oscillator model, we have observed that the degeneracy between the Rabi splittings associated with the symmetric and antisymmetric cavity modes is broken by the higher-order antiresonant terms in the Hamiltonian associated with the breakdown of the rotating wave approximation in the ultrastrong coupling regime. These results are in quantitative agreement with both experiment and transfer matrix modeling. The component cavities are characterized by Q factors around 12 and display a large vacuum Rabi splitting around 1.12 eV between the upper and lower polariton branches, which is about 52% of the excited state energy, thus indicating ultrastrong coupling in each individual cavity. This large splitting is due to the large oscillator strength of the neat dye glass. We have also observed large polariton-induced incidence-side asymmetry in reflection spectra in a coupled cavity pair with one cavity having no exciton.

I. INTRODUCTION

Light-matter interactions in optical cavities are being intensively studied, well beyond the laser concept and now encompassing both fundamental investigations and application in light emission, nonlinear optics, and quantum information [1–3]. Coupled microcavities introduce additional degrees of freedom, both for materials and the cavity interactions, and have attracted increasing attention. Quantum well based coupled inorganic microcavites (MCs) have been well studied for theory and optical devices [4–11]. Cavity polariton-induced splitting of excitonic states and optical reflection asymmetry were reported by Armitage *et al.* in quantum well based coupled inorganic MCs [6,7]. Some researchers analyzed the polariton-polariton interaction potentials using pump-probe degenerate scattering [9]. With the increasing degrees of freedom, these multiple microcavity systems have promising applications, such as angle-resonant stimulated polariton amplifiers and optical parametric oscillators [10,11].

To our knowledge, coupling between multiple cavities in the ultrastrong limit has not been observed in any material. We report here on such coupled cavities where we have observed in experiment and theory, the broken degeneracy between the Rabi splittings associated with the symmetric and antisymmetric cavity modes brought about by the departure from the rotating wave approximation.

Organic semiconductor-based single microcavities composed by high-Q or low-Q reflectors, exhibiting large vacuum Rabi splitting, have been particularly interesting as strong and ultrastrong exciton-photon coupling can be readily attained at room temperature [12–24]. In this framework, due to the specific excitonic property of organic materials, allowing the ultrastrong coupling regime with a large Rabi splitting to be reached, the demonstration of such coupled multiple organic

microcavities, each in the ultrastrong regime, suggests the potential for new physics and applications for tunable polariton-based devices operating at room temperature [25], with new concepts in quantum information being one example [26].

Here, we demonstrate coupling between a pair of ultrastrong exciton-photon coupled all-metal microcavities with low-Q value for each single cavity. The coupled cavities comprised two single exciton-photon coupled microcavities in the ultrastrong coupling regime. The organic material used within the microcavities is a well-studied molecular glass of an organic dye with large inhomogeneous absorption broadening. The large oscillator strength of the material is a key factor to reach the ultrastrong coupling regime [22]. The use of a neat molecular glass provides for a high number density for a large oscillator strength with high optical quality. Mixing a dye in a polymer matrix lowers the number density and therefore limits the oscillator strength, coupling, and, consequently, Rabi splitting, even though this kind of mixture might have a narrow linewidth [24].

This paper is organized as follows. In Sec. II, the experimental details of organic microcavities (OMCs) fabrication and various characterization methods are described. The experimental results are presented and discussed, and a modified theory for coupled OMCs is proposed in Sec. III. Conclusions and implications of this work are provided in Sec. IV.

II. EXPERIMENT

We have fabricated low-Q single cavity and double cavity microcavity polariton devices using metal mirrors enclosing a neat organic dye glass, DCDHF-6-V. Two types of coupled double cavities are studied: (a) symmetric cavities where both contain the exciton dye glass, and (b) asymmetric cavities where one is filled with DCDHF-6-V and one with a nonabsorbing polymer. Reflection spectra at various angles are used to characterize the cavities and coupling by determining the energies of the anticrossed levels. Results are compared
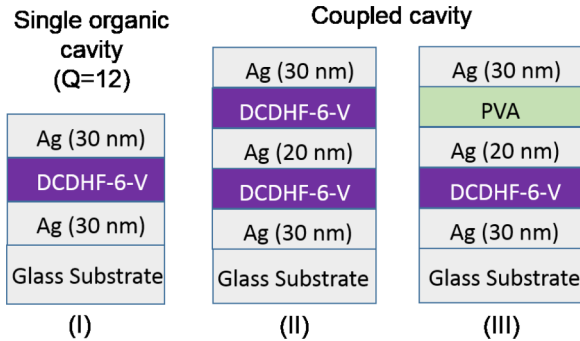
*bxl224@case.edu
†kds4@case.edu

FIG. 1. (Color online) Structures for single OMCs (I) and coupled OMCs (II) and (III). The transparent PVA film within cavity structure (III) works as a spacer layer.
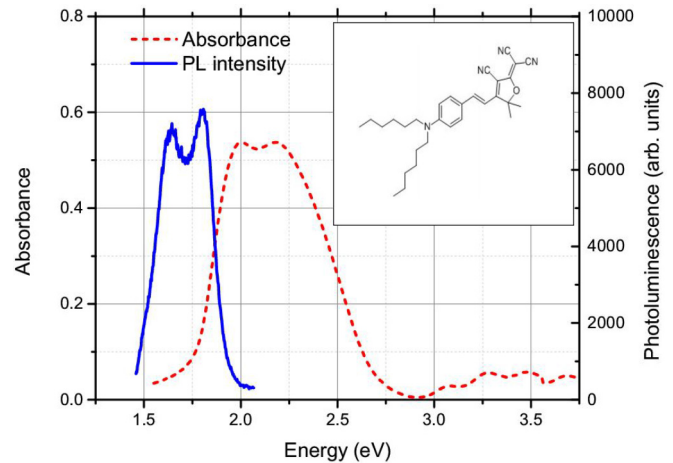

FIG. 2. (Color online) The absorbance (red curve) and photoluminescence emission (blue curve) spectra of a 90-nm-thick neat film of DCDHF-6-V. The inset shows the chemical structure of DCDHF-6-V.

with a four-state coupled model and optical transfer matrix simulations.

The organic dyes examined here are in the push-pull DCDHF class which we have previously used in a variety of optoelectronic applications [27–29]. Amongst these DCDHF dyes the specific substance DCDHF-6-V (CAS 634202-68-9) has been most thoroughly examined during our initial studies. For the single OMCs, films were deposited from toluene solution onto a thin (30 nm) silver film evaporated onto a 1-mm-thick glass substrate in vacuum at 10^{-7} Torr. DCDHF-6-V was spin cast on top of the metal film, and the thickness of the organic film was varied from 90 to 170 nm by adjusting the spin speed. Microcavity fabrication was completed by evaporating a second thin (30 nm) silver film on top of the organic layer. This process provided microcavities with low Q values around 12. For the coupled OMCs, a thinner (20 nm) silver layer was made in the center of microcavity structures. Figure 1 shows the structures for single OMCs (I) and coupled OMCs (II) and (III) we have studied. In structure III, polyvinyl alcohol (PVA) is an exciton-less transparent polymer film used to create an asymmetric coupled system for demonstrating optical asymmetry by illuminating the coupled cavity from its top and bottom.

The absorption spectra measurements of neat DCDHF-6-V film were carried out using a UV-Vis-NIR spectrophotometer, and photoluminescence emission spectra were measured by a spectrofluorometer. The organic microcavities were characterized by angularly resolved reflectivity measurements by using a spectroscopic ellipsometer at room temperature.

The reflectivity spectra for single and coupled microcavities studied have been theoretically calculated by transfer matrix simulation method [30,31]. Transfer matrix calculations were carried out using the complex index of refraction obtained by detailed modeling of spectroscopic ellipsometry data for each material.

III. RESULTS AND DISCUSSION

Figure 2 shows the room-temperature absorption and photoluminescence emission spectra from a 90-nm-thick neat film of DCDHF-6-V spin cast onto a glass substrate. The Stokes shift can be observed, and the FWHM for the transition at 2.16 eV is 0.58 eV, and the strong inhomogeneous broadening

of the excitonic resonance results from the disorder inherent in the organic glass (DCDHF-6-V) [32].

A. Single organic microcavity

The cavity mode can be tuned to be resonant with the exciton state by varying the angle of incidence, as the wave vector **k** is varied. Figures 3(a) and 3(b) show the variation in room-temperature reflectivity spectra as the photon mode is angle tuned through the exciton mode energy with TM and TE polarized light, respectively. At each angle, two reflectivity dips, corresponding to the cavity polariton states, are observed, and the shift of energetic positions of the cavity polariton states can be seen clearly as the angle of incidence is varied. To represent the experimentally measured dispersion more directly, contour plots of the angle-resolved reflectivity (**R**) are shown in Fig. 4(a) for TM and Fig. 4(b) for TE polarization. The dispersion shown in Figs. 4(a) and 4(b) exhibits widely separated anticrossed states characteristic of a strongly coupled exciton-polariton. Two cavity polariton branches, upper polariton (UP) and lower polariton (LP), are observed near the point where the dispersions of the uncoupled cavity mode (dashed white curve) and excited state (solid blue line) cross. At this point, the vacuum Rabi splitting energy ($\hbar\Omega_R$) as the minima of the energy difference between UP and LP, is obtained. The dispersion relations of the cavity polariton calculated using the transfer matrix reflectivity model are shown by the dashed black curves, which precisely agree with the measurement results. The horizontal blue line is the exciton transition energy of DCDHF-6-V. This energy is angle independent and so is expected to give the resonance energy for the coupled exciton-photon system [12]. Comparing these two contour plots, the polariton dispersion of the TM modes is flatter than that of the TE modes consistent with polarization dependence of the bare cavity photon dispersion [22] shown as the dashed white curves in Figs. 4(a) and 4(b). The resonance between photon and exciton occurs at around 25° and 15° for TM and TE polarization, respectively. The measurement results give the same $\hbar\Omega_R$ value of 1.12 eV for both TM and TE polarization.
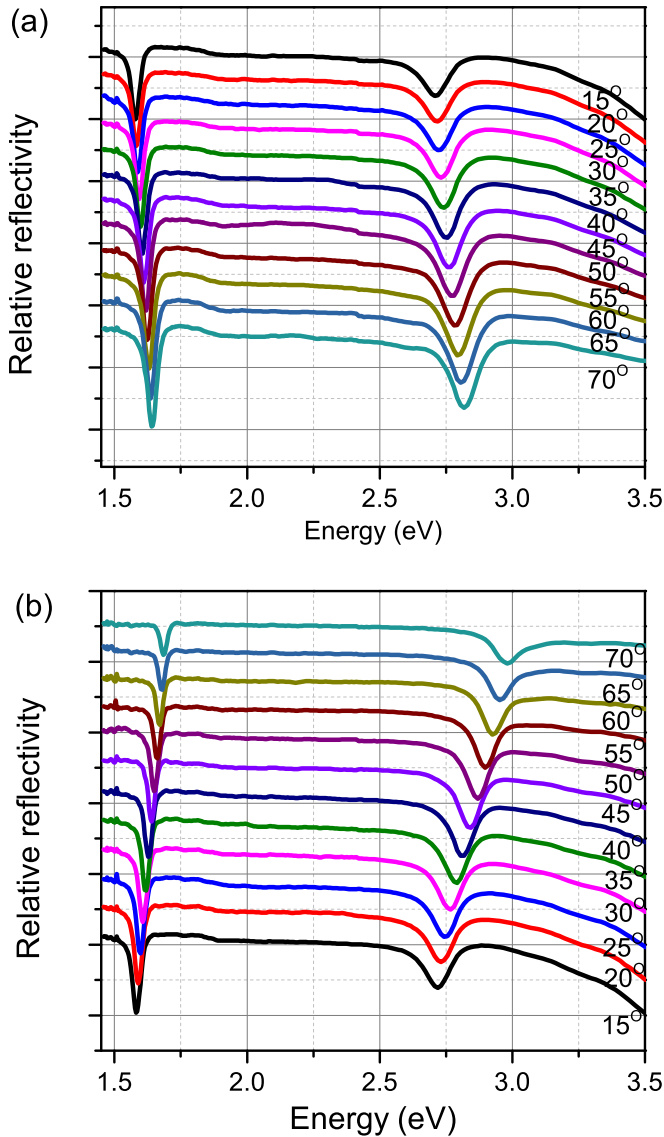
FIG. 3. (Color online) Angularly resolved reflectivity spectra for an organic microcavity containing a 140-nm-thick DCDHF-6-V film for TM (a) and TE (b) polarization. The spectra for different measurement angles (indicated in the figure) have been displaced vertically for clarity.
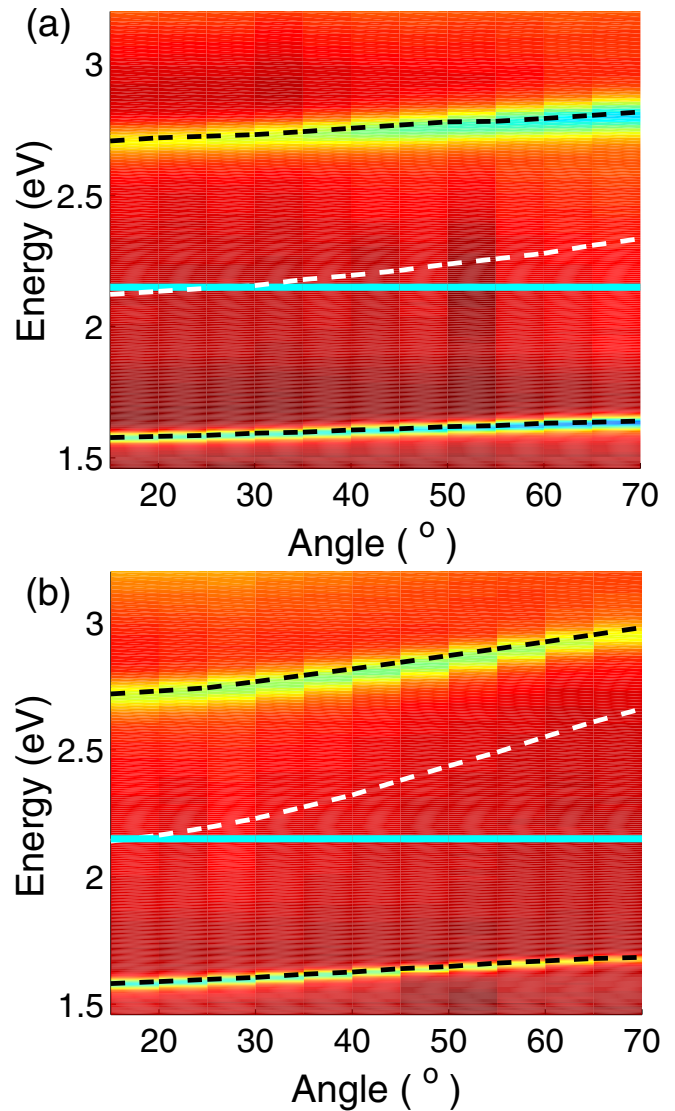

FIG. 4. (Color online) Angle-resolved reflectivity maps of the 140-nm-thick microcavity. The spectra are shown for TM (a) and TE (b) polarization. The dashed black curves, which are obtained by transfer matrix calculation, trace the positions of the reflectivity minima that correspond to the UP and LP branches. The dashed white curve is the dispersion of bare cavity mode, and the blue line shows the DCDHF-6-V exciton transition energy.

To connect better to the underlying physics, we plot the dispersion as a function of the wave vector **k**, shown in Fig. 5(a) for TM and (b) for TE polarization. The in-plane wave vector $\mathbf{k}_{\parallel}$ is related to the incident angle θ and wavelength λ of the incident light through the relation $\mathbf{k}_{\parallel} = \sin\theta(2\pi/\lambda)$ [14]. The measured anticrossing dispersions as a function of the wave vector **k** also give the same $\hbar\Omega_R$ value of 1.12 eV for both TM and TE polarization.

Next, we can examine the calculated vacuum Rabi splitting energy $\hbar\Omega_R$ with a simple classical model. The coupling parameter between a dielectric material and an optical cavity is given as follows [33]:

$$g_0 = \left(\frac{N\mu_{12}^2\omega}{2\epsilon_0 V_0 \hbar}\right)^{1/2}, \qquad (1)$$

where ϵ_0 is the dielectric constant of organic material, $\frac{N}{V_0}$ is the molecular number density, $E_0 = \hbar\omega$ is the transition energy, and $\mu_{12} \equiv \langle \Psi_1|e\vec{r}|\Psi_2\rangle$ is the electric dipole matrix element of the transition. Generally, in the classical oscillator model, the vacuum Rabi-splitting energy $\hbar\Omega_R$ in an OMC can be expressed as [34]

$$\hbar\Omega_R = 2\left[(\hbar g_0)^2 - \frac{1}{4}(\delta_{ex} - \delta_{cav})^2\right]^{1/2}, \qquad (2)$$

where δ_{ex} and δ_{cav} are the uncoupled excited state and cavity half widths (HWFM), respectively. The parameters shown in Eqs. (1) and (2) for the (DCDHF-6-V)-filled OMC are given in Table I. The calculated Rabi splitting using Eqs. (1) and (2) along with the experimentally determined oscillator strength
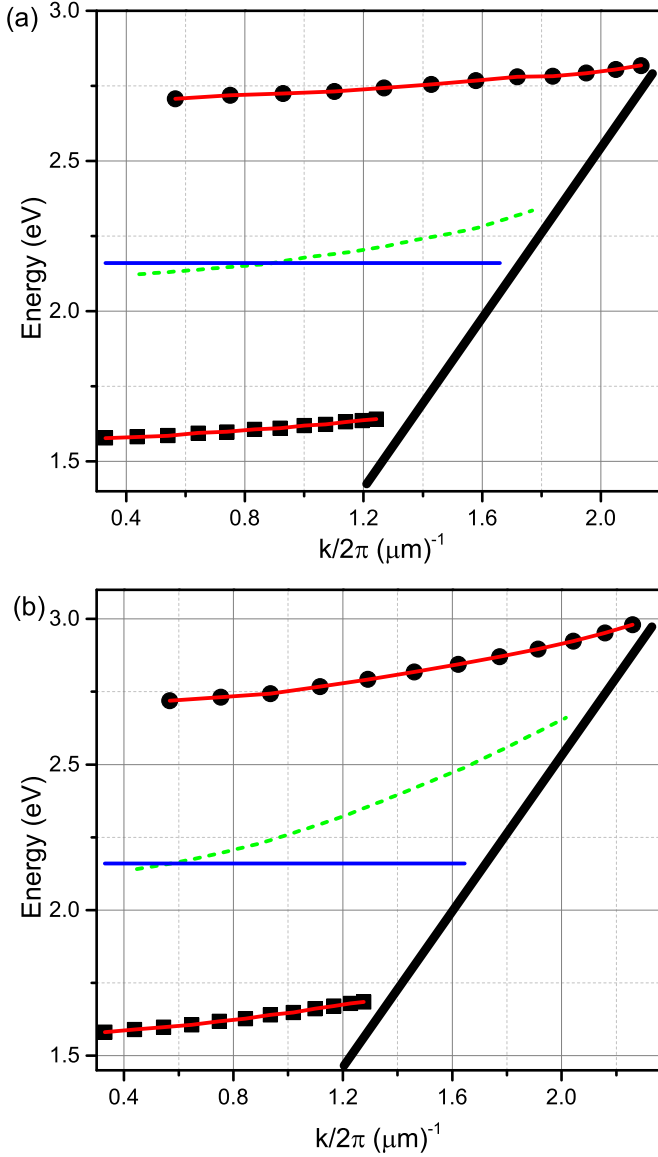
FIG. 5. (Color online) Anticrossing dispersions as a function of the wave vector for TM (a) and TE (b) polarization. Circles and squares are measurement data, and the red curves are obtained by transfer matrix calculation. The dashed green curve is the dispersion of bare cavity mode, and the blue line shows the DCDHF-6-V exciton transition energy. The diagonal black line on the right of the plot signifies the maximum scan angle.

and spectral widths is obtained as 1.118 eV, which is in excellent agreement with the experimental value of 1.120 eV, even though Eq. (2) applies to homogeneously broadened spectra. These results are consistent with the sharp falloff of

TABLE I. Parameter values in Eqs. (1) and (2) for an OMC filled with a 140 nm DCDHF-6-V film.

$\frac{N}{V_0}$ (cm^{-3})	μ_{12} (D)	$\hbar\omega$ (eV)	δ_{ex} (eV)	δ_{cav} (eV)	$\hbar g_0$ (eV)	$(\hbar\Omega_R)_{\text{calc}}$ (eV)	$(\hbar\Omega_R)_{\text{expt.}}$ (eV)
1.8×10^{21}	7.3	2.16	0.29	0.23	0.56	1.118	1.120

the inhomogeneously broadened spectra where the coherence of the inhomogeneously broadened dipoles is maintained [35]. This is in keeping with the narrow polariton linewidths observed and with the observations of Gambino *et al*. [24]. There are three main contributions to the large Rabi splitting of the (DCDHF-6-V)-filled OMC: (1) the large number density of the material as a neat organic glass; (2) the large electric dipole matrix element of the transition due to the broad absorption spectrum and high exciton oscillator strength; and (3) the similar linewidths between the uncoupled exciton and cavity mode. The first two factors give rise to a large coupling parameter $\hbar g_0$ around 0.56 eV, thus a large vacuum Rabi splitting, because $\hbar\Omega_R$ depends on the oscillator strength determined from the energy-integrated absorption rather than on just the magnitude of the absorption peak [24,36].

B. Coupled organic microcavity

For the coupled OMCs with the structure shown in Fig. 1(II), a series of TM polarized reflectivity spectra taken at room temperature is shown in Fig. 6(a). For each angle, four reflectivity dips corresponding to the cavity polariton states, are observed, and the energetic positions of the dips shift as the angle of incidence is varied. Extracting the energetic positions of those reflectivity minima, four cavity polariton branches, indicated as UP, MP1, MP2, and LP branches, can be seen in Fig. 6(b). According to the measurement results, anticrossing between UP and MP2 occurs at around 15° with a vacuum Rabi splitting $\hbar\Omega_{R1}$ of 1.11 eV, while anticrossing between MP1 and LP occurs at around 40° with a vacuum Rabi splitting $\hbar\Omega_{R2}$ of 1.08 eV. The anticrossing occurs at different angles (different wave vector **k**), which is consistent with the observation by Armitage *et al*. for the strongly coupled inorganic MCs, and this is due to the splitting between symmetric and antisymmetric cavity modes [6]. However, the inequality of these two splittings is inconsistent with the prediction of the classical four-oscillator coupled model proposed by Armitage *et al*. for the strong coupling regime. For the coupled OMCs in the ultrastrong coupling regime, a modified four-oscillator coupled model is now examined that takes into account the antiresonant Hamiltonian terms for the interacting system beyond the rotating wave approximation.

1. Modified four-oscillator coupled model for coupled OMCs

First, the optical fields in the cavities couple yield symmetric and antisymmetric cavity modes, and the coupled cavity energies can be obtained via [6]

$$\begin{bmatrix} E_c & V_0 \\ V_0 & E_c \end{bmatrix}\begin{bmatrix} \alpha \\ \beta \end{bmatrix} = E\begin{bmatrix} \alpha \\ \beta \end{bmatrix}, \quad (3)$$

where E_c is the energy of the uncoupled cavity modes and V_0 is the optical coupling parameter between the cavities. The energies of the symmetric and antisymmetric coupled cavity modes are given by $E_S = E_c + V_0$, $E_{AS} = E_c - V_0$.

Second, the exciton states in the two separate cavities also form symmetric and antisymmetric combinations (ψ_S, ψ_{AS}) given as $\psi_S = (\phi_1 + \phi_2)/2$ and $\psi_{AS} = (\phi_1 - \phi_2)/2$, where ϕ_1 and ϕ_2 are the single exciton wave functions in the two cavities [6,37].
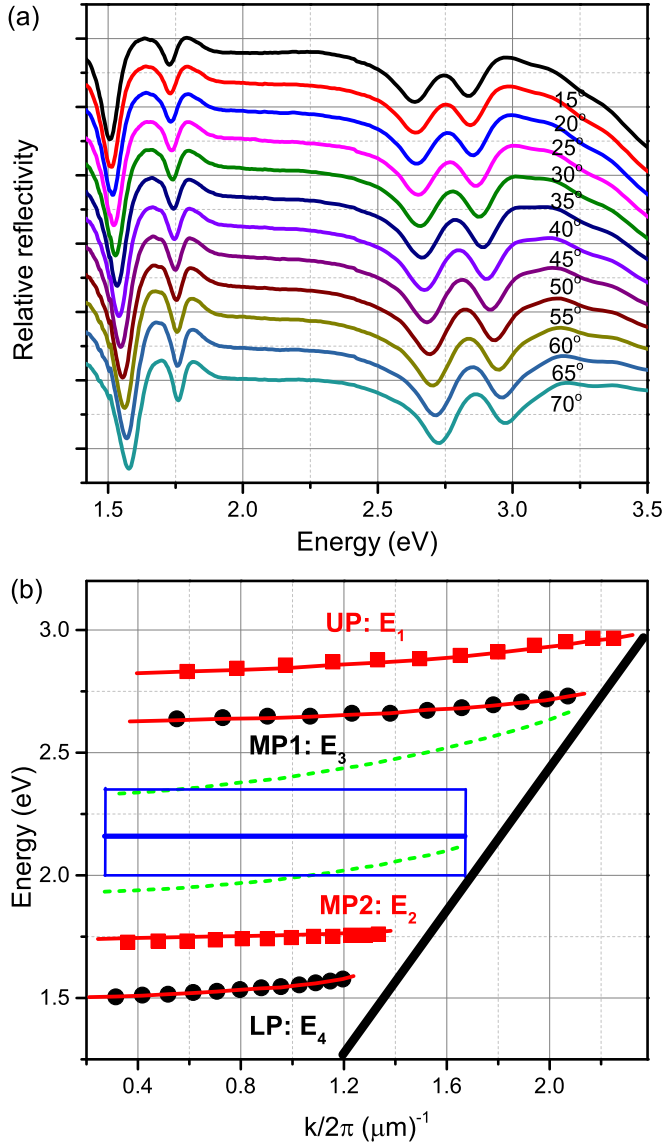
FIG. 6. (Color online) (a) Angularly resolved reflectivity spectra for a coupled OMC containing two 140-nm-thick DCDHF-6-V layers for TM polarization. The spectra for different measurement angles (indicated in the figure) have been displaced vertically for clarity. (b) Energetic positions of reflectivity dips plotted as a function of the wave vector. Experimental data are shown as circles and squares, and the solid red curves are obtained by transfer matrix calculation. The dashed green curves are the dispersion of bare-cavity symmetric and antisymmetric modes. The blue rectangular box shows inhomogeneous broadening of excitonic resonance of DCDHF-6-V. The diagonal black line on the right of the plot signifies the maximum scan angle.

Third, the symmetric coupled cavity mode couples to the symmetric exciton state ψ_S, and the antisymmetric coupled cavity mode couples to the antisymmetric exciton state ψ_{AS} via the equation which describes the eigenvalues of the Hopfield Hamiltonian of the interacting system [24,38,39]:

$$\left(E_{cav}^2 - E^2\right)\left(\hat{E}_{ex}^2 - E^2\right) = \beta^2 E_{ex}^2 E_{cav}^2, \tag{4}$$

where E_{ex} is the exciton energy, $\beta = \hbar\Omega_R/E_{ex}$, and $\hat{E}_{ex}^2 = E_{ex}^2 + \beta^2 E_{ex}^2$. E_{cav} describes the energy dispersion of the cavity mode; for the coupled cavities, E_{cav} can be described as $E_S = E_c + V_0$, $E_{AS} = E_c - V_0$. Thus, for the coupled microcavities, taking into account the antiresonant Hamiltonian terms, the polariton energies can be described via

$$\left(E_{S/AS}^2 - E^2\right)\left(E_{ex}^2 + \beta^2 E_{ex}^2 - E^2\right) = \beta^2 E_{ex}^2 E_{S/AS}^2. \tag{5}$$

If β is relatively small corresponding to the strong coupling, the above equation can be approximated as

$$(E_{S/AS} - E)(E_{ex} - E) = V_1^2, \tag{6}$$

where we define $V_1^2 = \frac{1}{4}\beta^2 E_{ex}E_{S/AS}$, which is the coupling parameter between exciton and cavity modes. The above equations are the result of the classical four-oscillator coupled model, and the solutions for polariton eigenvalues at resonance (namely, $E_c = E_{ex}$) are given as

$$E_{1,2} = \frac{1}{2}\left(2E_{ex} + V_0 \pm \sqrt{V_0^2 + 4V_1^2}\right)$$
$$E_{3,4} = \frac{1}{2}\left(2E_{ex} - V_0 \pm \sqrt{V_0^2 + 4V_1^2}\right). \tag{7}$$

At resonance conditions, $\hbar\Omega_{R1} = \Delta E_{12} = \Delta E_{34} = \hbar\Omega_{R2} = \sqrt{V_0^2 + 4V_1^2}$, and this relation can only hold when the small-β condition is satisfied.

For the ultrastrong coupling regime, β is significant, thus, the polariton eigenvalues at resonance conditions can be derived from Eq. (5):

$$E_{1,2}^2 = \pm\frac{1}{2}\sqrt{\left[E_{ex}^2 + E_{SR}^2 + (\hbar\Omega_{R1})^2\right]^2 - 4E_{ex}^2 E_{SR}^2}$$
$$+ \frac{1}{2}\left[E_{ex}^2 + E_{SR}^2 + (\hbar\Omega_{R1})^2\right],$$

$$E_{3,4}^2 = \pm\frac{1}{2}\sqrt{\left[E_{ex}^2 + E_{ASR}^2 + (\hbar\Omega_{R2})^2\right]^2 - 4E_{ex}^2 E_{ASR}^2}$$
$$+ \frac{1}{2}\left[E_{ex}^2 + E_{ASR}^2 + (\hbar\Omega_{R2})^2\right], \tag{8}$$

where $E_{SR} = E_{ex} + V_0$, $E_{ASR} = E_{ex} - V_0$ at resonance conditions. According to Eq. (8), we can derive that $\hbar\Omega_{R1} = \Delta E_{12} = f[(\hbar\Omega_{R1})^2, E_{SR}^2]$, $\hbar\Omega_{R2} = \Delta E_{34} = f[(\hbar\Omega_{R2})^2, E_{ASR}^2]$, which could not guarantee that the equality $\hbar\Omega_{R1} = \hbar\Omega_{R2}$ always holds. From the measurement results, anticrossing between UP and MP2 occurs at around 15°, and the measured vacuum Rabi splitting $\hbar\Omega_{R1} = E_1 - E_2 = 2.83 - 1.72 = 1.11$ eV, and the calculated $\hbar\Omega_{R1}$ from Eq. (8) is 1.106 eV. Anticrossing between MP1 and LP occurs at around 40°, and the measured vacuum Rabi splitting $\hbar\Omega_{R2} = E_3 - E_4 = 2.64 - 1.56 = 1.08$ eV, and the calculated $\hbar\Omega_{R2}$ from Eq. (8) is 1.05 eV. The strong quantitative agreement between the measurement and calculated results confirm that the modified four-oscillator coupled model can describe the dispersion of cavity polariton states and permit a good physical understanding of the on-resonance behavior for the coupled microcavities in the ultrastrong coupling regime. The observed broken degeneracy between the UP-MP2 and MP1-LP Rabi splittings is a signature of coupling between the double exciton-photon ultrastrong coupled cavities and
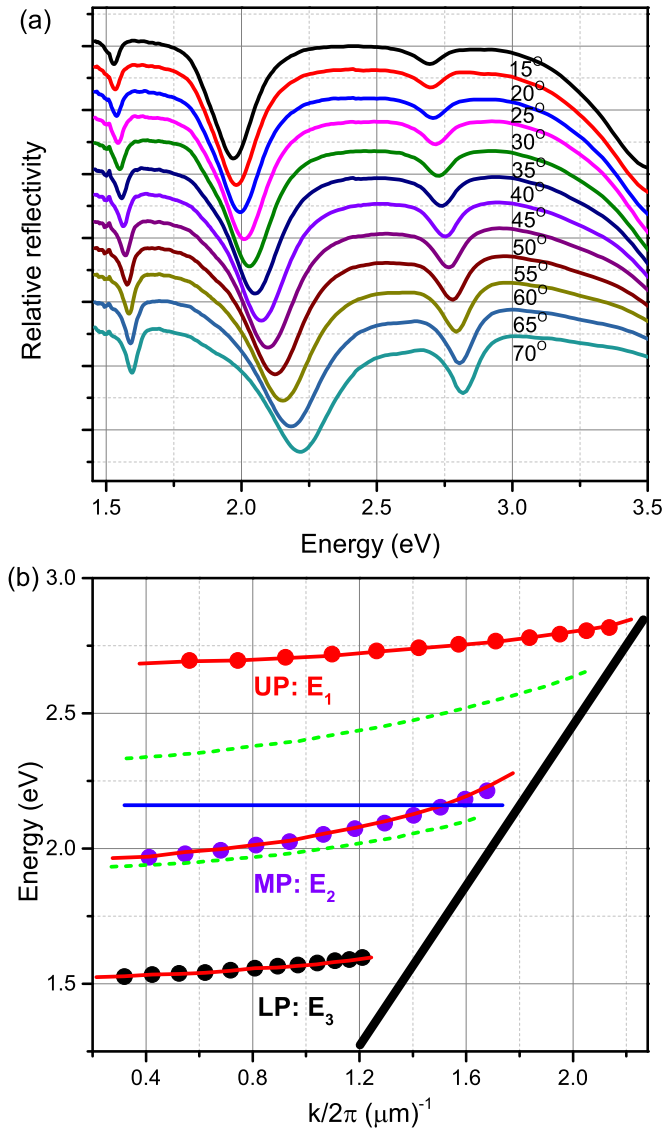
FIG. 7. (Color online) (a) Angularly resolved reflectivity spectra for a coupled OMC, which has a structure shown in Fig. 1(III), containing a 140-nm-thick DCDHF-6-V film and a 140-nm-thick PVA film for TM polarization. The coupled cavity is illuminated from its top. (b) Energetic positions of reflectivity dips plotted as a function of the wave vector. Experimental data are shown as circles, and the solid red curves are obtained by transfer matrix calculation. The dashed green curves are the dispersion of bare-cavity symmetric and antisymmetric modes. The blue line is the DCDHF-6-V exciton transition energy. The diagonal black line on the right of the plot signifies the maximum scan angle.
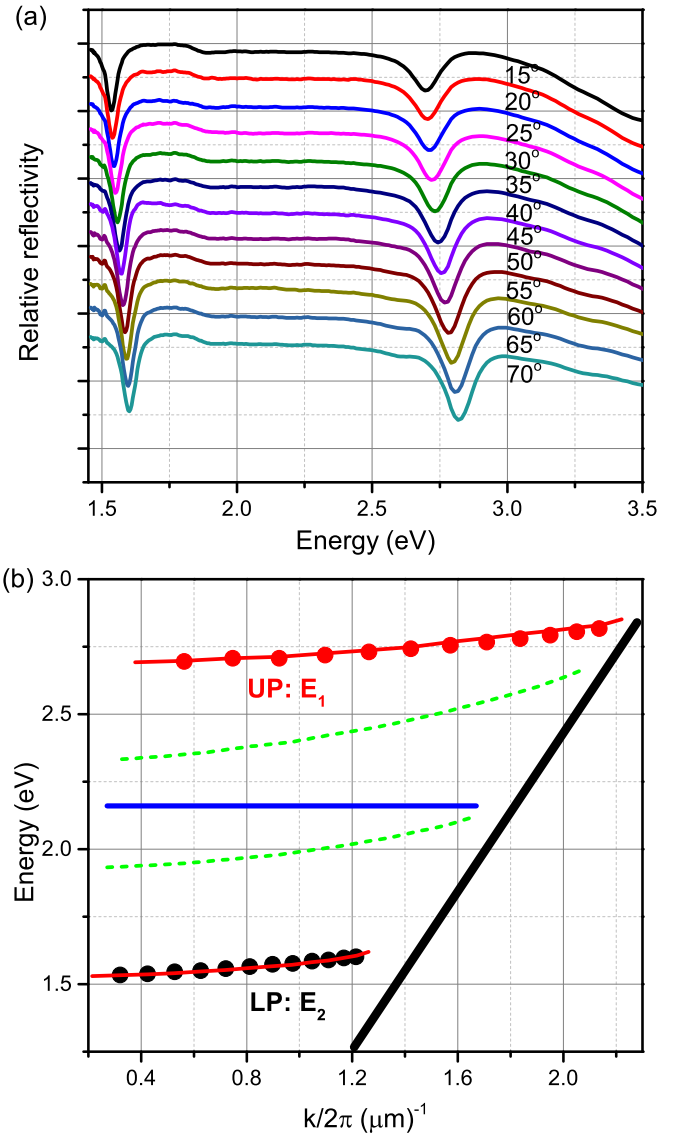
FIG. 8. (Color online) (a) Angularly resolved reflectivity spectra for a coupled OMC, which has a structure shown in Fig. 1(III), containing a 140-nm-thick DCDHF-6-V film and a 140-nm-thick PVA film for TM polarization. The coupled cavity is illuminated from its bottom. (b) Energetic positions of reflectivity dips plotted as a function of the wave vector. Experimental data are shown as circles, and the solid red curves are obtained by transfer matrix calculation. The dashed green curves are the dispersion of bare-cavity symmetric and antisymmetric modes. The blue line is the DCDHF-6-V exciton transition energy. The diagonal black line on the right of the plot signifies the maximum scan angle.

the higher-order antiresonant terms beyond the rotating wave approximation.

2. Polariton-induced optical asymmetry in coupled OMCs

For the coupled OMCs with the structure shown in Fig. 1(III), the angle-resolved reflectivity spectra taken for TM polarization at room temperature are shown in Figs. 7(a) and 8(a) when the coupled microcavity is illuminated from its top and bottom, respectively. In Fig. 7(a), three reflectivity dips corresponding to three cavity polariton states (UP, MP,

and LP), can be seen for each angle of incidence when the coupled microcavity is illuminated from its top. The energetic positions of cavity polariton states shift as the angle, thus the wave vector, is varied, consistent with anticrossing dispersion, which is shown in Fig. 7(b). At resonance at ∼20°, the splitting between UP and MP is 0.70 eV, while the splitting between LP and MP is 0.44 eV. When the reflectivity measurements are taken by illuminating the coupled cavity from its bottom, only two reflectivity dips, which correspond to UP and LP states, are observed for each angle of incidence, and the central mode

(MP) is unobservable. The anticrossing dispersion is shown in Fig. 8(b), and the splitting between UP and LP is 1.12 eV at resonance at $\sim 50^{\circ}$.

According to measurement results and the discussions above, the central mode is unobservable when light is incident on the cavity containing DCDHF-6-V film. In contrast, when light is incident on the cavity containing the spacer layer of PVA film, the central mode (MP) is always observable and strong, and more photonlike dispersive than the other two modes (UP and LP). This optical asymmetry in the reflectivity spectra is induced by the cavity polariton, and similar results have been reported for the coupled inorganic microcavities [7]. Armitage *et al.* proposed a three-coupled oscillator model composed of the optical modes from two cavities and the excitonic states, explaining that whether the central mode (MP) is observable (bright) or not (dark) depends on the direction of observation, consistent with the eigenstates of the system. Our results showing very large splittings at room-temperature and low-Q cavities indicate a new regime for observation of this asymmetry. These results may provide applications for fast-response optical switches by converting dark modes to bright ones in asymmetric coupled OMCs [7].

IV. CONCLUSION

Here, we have demonstrated coupling between a pair of ultrastrong light-matter coupled single microcavities, which are constructed from low-Q all-metal mirrors filled with the glass forming dye of DCDHF-6-V at room temperature. Because of the nonlinear coupling describing the ultrastrong limit, the degeneracy between the Rabi splittings associated with symmetric and asymmetric cavity modes is broken by the antiresonant terms beyond the rotating wave approximation. This is in quantitative agreement with a modified four-oscillator coupled model. The large vacuum Rabi splitting, which is an appreciable fraction of the excited state energy of material, and the anticrossing dispersion are the most significant features for the ultrastrong coupling regime. Furthermore, we have observed polariton-induced optical asymmetry in the reflectivity spectra of coupled organic microcavities having much larger splittings than those of coupled inorganic microcavities. These results are very promising for the study of light-matter interaction physics, and could lead to applications of coupled organic multiple microcavities in the ultrastrong light-matter coupling regime for the constituent microcavities at room temperature, for example in organic microcavity light-emitting diodes, where the coupling effect can narrow the linewidth of emission [23]. The coupled cavity is also an interesting system for realizing photon blockades in the ultrastrong coupling regime [40].

[1] M. Mazzeo, A. Genco, S. Gambino, D. Ballarini, F. Mangione, O. Di Stefano, S. Patanè, S. Savasta, D. Sanvitto, and G. Gigli, Appl. Phys. Lett. **104**, 233303 (2014).

[2] S. Kéna-Cohen and S. R. Forrest, Nat. Photonics **4**, 371 (2010).

[3] T. H. Stievater, Xiaoqin Li, D. G. Steel, D. Gammon, D. S. Katzer, D. Park, C. Piermarocchi, and L. J. Sham, Phys. Rev. Lett. **87**, 133603 (2001).

[4] R. P. Stanley, R. Houdré, U. Oesterle, M. Ilegems, and C. Weisbuch, Appl. Phys. Lett. **65**, 2093 (1994).

[5] M. S. Skolnick, T. A. Fisher, and D. M. Whittaker, Semicond. Sci. Technol. **13**, 645 (1998).

[6] A. Armitage, M. S. Skolnick, V. N. Astratov, D. M. Whittaker, G. Panzarini, L. C. Andreani, T. A. Fischer, J. S. Roberts, A. V. Kavokin, M. A. Kaliteevski, and M. R. Vladimirova, Phys. Rev. B **57**, 14877 (1998).

[7] A. Armitage, M. S. Skolnick, A. V. Kavokin, D. M. Whittaker, V. N. Astratov, G. A. Gehring, and J. S. Roberts, Phys. Rev. B **58**, 15367 (1998).

[8] C. Diederichs and J. Tignon, Appl. Phys. Lett. **87**, 251107 (2005).

[9] T. Lecomte, D. Taj, A. Lemaitre, J. Bloch, C. Delalande, J. Tignon, and P. Roussignol, Phys. Rev. B **89**, 155308 (2014).

[10] P. G. Savvidis, J. J. Baumberg, R. M. Stevenson, M. S. Skolnick, D. M. Whittaker, and J. S. Roberts, Phys. Rev. Lett. **84**, 1547 (2000).

[11] C. Diederichs, J. Tignon, G. Dasbach, C. Ciuti, A. Lematre, J. Bloch, P. Roussignol, and C. Delalande, Nature (London) **440**, 904 (2006).

[12] D. G. Lidzey, D. D. C. Bradley, M. S. Skolnick, T. Virgili, S. Walker, and D. M. Whittaker, Nature (London) **395**, 53 (1998).

[13] D. G. Lidzey, D. D. C. Bradley, A. Armitage, S. Walker, and M. S. Skolnick, Science **288**, 1620 (2000).

[14] P. A. Hobson, W. L. Barnes, D. G. Lidzey, G. A. Gehring, D. M. Whittaker, M. S. Skolnick, and S. Walker, Appl. Phys. Lett. **81**, 3519 (2002).

[15] D. G. Lidzey, A. M. Fox, M. D. Rahn, M. S. Skolnick, V. M. Agranovich, and S. Walker, Phys. Rev. B **65**, 195312 (2002).

[16] L. G. Connolly, D. G. Lidzey, R. Butte, A. M. Adawi, D. M. Whittaker, M. S. Skolnick, and R. Airey, Appl. Phys. Lett. **83**, 5377 (2003).

[17] R. F. Oulton, N. Takada, J. Koe, P. N. Stravrinou, and D. D. C. Bradley, Semicond. Sci. Technol. **18**, S419 (2003).

[18] R. J. Holmes and S. R. Forrest, Phys. Rev. Lett. **93**, 186404 (2004).

[19] J. Wenus, L. G. Connolly, D. M. Whittaker, M. S. Skolnick, and D. G. Lidzey, Appl. Phys. Lett. **85**, 5848 (2004).

[20] R. J. Holmes and S. R. Forrest, Phys. Rev. B **71**, 235203 (2005).

[21] T. Schwartz, J. A. Hutchison, C. Genet, and T. W. Ebbesen, Phys. Rev. Lett. **106**, 196405 (2011).

[22] S. Kéna-Cohen, S. A. Maier, and D. D. C. Bradley, Adv. Opt. Mater. **1**, 827 (2013).

[23] S. Wang, T. Chervy, J. George, J. A. Hutchison, C. Genet, and T. W. Ebbesen, J. Phys. Chem. Lett. **5**, 1433 (2014).

[24] S. Gambino, M. Mazzeo, A. Genco, O. Di Stefano, S. Savasta, S. Patanè, D. Ballarini, F. Mangione, G. Lerario, D. Sanvitto, and G. Gigli, ACS Photonics **1**, 1042 (2014).

[25] S. Stelitano, G. D. Luca, S. Savasta, L. M. Scolaro, and S. Patané, Appl. Phys. Lett. **95**, 093303 (2009).

[26] S. Portolan, L. Einkemmer, Z. Vörös, G. Weihs, and P. Rabl, New J. Phys. **16**, 063030 (2014).

[27] O. Ostrovherkhova, W. E. Moerner, M. He, and R. J. Twieg, Appl. Phys. Lett. **82**, 3602 (2003).

[28] W. E. Moerner, R. J. Twieg, D. Kline, and M. He, U. S. Pat. Appl. Publ. **A1**, US20050009109 (2005).

[29] P. D. Cunningham, N. N. Valdes, F. A. Vallejo, L. M. Hayden, B. Polishak, X. Zhou, J. Luo, A. K.-Y. Jen, J. C. Williams, and R. J. Twieg, J. Appl. Phys. **109**, 043505 (2011).

[30] P. Yeh, *Optical Waves in Layered Media* (Wiley-Interscience, New York, 2005).

[31] B. Valle, S. Loser, J. W. Hennek, V. DeGeorge, C. Klosterman, J. H. Andrews, K. D. Singer, and T. J. Marks, Opt. Express **20**, A954 (2012).

[32] V. M. Agranovich, M. Litinskaia, and D. G. Lidzey, Phys. Rev. B **67**, 085311 (2003).

[33] M. Fox, *Quantum Optics: An Introduction* (Oxford University Press, New York, 2005).

[34] V. Savona, L. C. Andreani, P. Schwendimann, and A. Quatropani, Solid State Commun. **93**, 733 (1995).

[35] I. Diniz, S. Portolan, R. Ferreira, J. M. Gérard, P. Bertet, and A. Auffèves, Phys. Rev. A **84**, 063810 (2011).

[36] R. Houdré, R. P. Stanley, and M. Ilegems, Phys. Rev. A **53**, 2711 (1996).

[37] G. Panzarini, L. C. Andreani, A. Armitage, D. Baxter, M. S. Skolnick, V. N. Astratov, J. S. Roberts, A. V. Kavokin, M. R. Vladimirova, and M. A. Kaliteevski, Phys. Rev. B **59**, 5082 (1999).

[38] Y. Todorov, A. M. Andrews, R. Colombelli, S. De Liberato, C. Ciuti, P. Klang, G. Strasser, and C. Sirtori, Phys. Rev. Lett. **105**, 196402 (2010).

[39] J. J. Hopfield, Phys. Rev. **112**, 1555 (1958).

[40] A. Ridolfo, M. Leib, S. Savasta, and M. J. Hartmann, Phys. Rev. Lett. **109**, 193602 (2012).